Editors' Suggestion

Exciton Photoemission from a Ground State of a Solid: $Ta_2Pd_3Te_5$

Siwon Lee,[1,2] Kyung-Hwan Jin,[2,3] SeongJin Kwon,[1,2] Hyunjin Jung,[1,2] Choongjae Won,[4,5] Sang-Wook Cheong,[5,6] Gil Young Cho,[1,7] Jaeyoung Kim,[2] and Han Woong Yeom[1,2,*]

[1]*Department of Physics, Pohang University of Science and Technology (POSTECH), Pohang 37673, Republic of Korea*
[2]*Center for Artificial Low Dimensional Electronic Systems, Institute for Basic Science (IBS), Pohang 37673, Republic of Korea*
[3]*Department of Physics and Research Institute for Materials and Energy Sciences, Jeonbuk National University, Jeonju, 54896, Republic of Korea*
[4]*Max Planck POSTECH/Korea Research Initiative, Center for Complex Phase of Materials, Pohang, 37673, Republic of Korea*
[5]*Laboratory of Pohang Emergent Materials, Pohang Accelerator Laboratory, Pohang, 37673, Republic of Korea*
[6]*Keck Center for Quantum Magnetism and Department of Physics and Astronomy, Rutgers University, New Jersey 08901-8554, USA*
[7]*Department of Physics, Korea Advanced Institute of Science and Technology, Daejeon, 34141, Republic of Korea*

(Received 6 March 2025; revised 30 May 2025; accepted 7 August 2025; published 9 September 2025)

Excitons are bosonic quasiparticles with a variety of applications in optoelectronics, photosynthesis, and dissipationless informatics, and their lifetime can become sufficiently long to form a quantum condensate. While exciton condensation has been predicted to occur as a ground state of a solid, so-called an excitonic insulator, whose material realization has been elusive. Here we report the observation of direct photoemission signals from excitons in a ground state of a very recent excitonic insulator candidate $Ta_2Pd_3Te_5$ below its metal-insulator transition temperature using orbital-selective angle-resolved photoemission spectroscopy. It is confirmed that the excitons have a lower energy than the valence band maximum to possibly drive the phase transition. This measurement further discloses the size and the unusual odd parity of the exciton wave function. The present finding opens an avenue toward applications of coherent excitons in solid systems and searching for exotic quantum phases of exciton condensates.

DOI: 10.1103/5kd3-trkg

Excitons represent bound states of electrons and holes formed by Coulomb attraction, which play important roles in diverse photoexcitation processes from semiconductor optical properties and photovoltaics to photosynthesis [1–10]. An exciton can also be spontaneously formed as a ground state of a solid when the exciton binding energy exceeds the band gap; a single-electron band gap is replaced by a manybody excitonic gap below a transition temperature T_c and excitons form a quantum condensate. This was predicted to occur in a semimetal and a small-gap semiconductor with poorly screened Coulomb interaction to minimize the band gap with maximized Coulomb attraction [11–24]. The evidence of the exciton condensation, a transition into an excitonic insulator, was recently reported in monolayers of transition metal dichalcogenides [19–24]. However, the confirmation of an excitonic insulator remains elusive in a 3D crystalline form of solids in spite of substantial recent efforts devoted particularly to transition metal chalcogenide materials such as $TiSe_2$ [25–28] and Ta_2NiSe_5 [29–33]. The major challenge has been the inevitable coupling of electronic and lattice degrees of freedom, which would induce substantial structural changes in a putative excitonic gap opening. The major driving force of the transition thus becomes ambiguous with both excitonic and structural contributions entangled [25–33].

On the other hand, recent works demonstrated that excitons manifest themselves as a characteristic photoemission signal [34–42]. When it absorbs an incoming photon of sufficient energy, an exciton emits a photoelectron, leaving a hole within the solid [Fig. 1(a)]. The exciton photoelectron spectral function is given as a convolution of the exciton wave function and that of conduction band electrons [43] as well established in pump-probe photoemission experiments for excited state excitons within band gaps of semiconductors [34–42]. While applying a similar method is not trivial in an excitonic insulator due to an energy overlap of excitons with valence bands, a recent work successfully isolated the characteristic exciton photoemission signal in Ta_2NiSe_5 utilizing orbital selection rules of photoemission [44]. However, very intriguingly, the exciton photoemission signal was observed only above T_c. This was interpreted to indicate the spontaneous formation of many incoherent excitons above T_c and, although not completely clear yet, the exciton photoemission signal may be suppressed by the strong exciton-lattice interaction below T_c. This made the confirmation of excitons in an

*Contact author: yeom@postech.ac.kr

Published by the American Physical Society under the terms of the Creative Commons Attribution 4.0 International license. Further distribution of this work must maintain attribution to the author(s) and the published article's title, journal citation, and DOI.

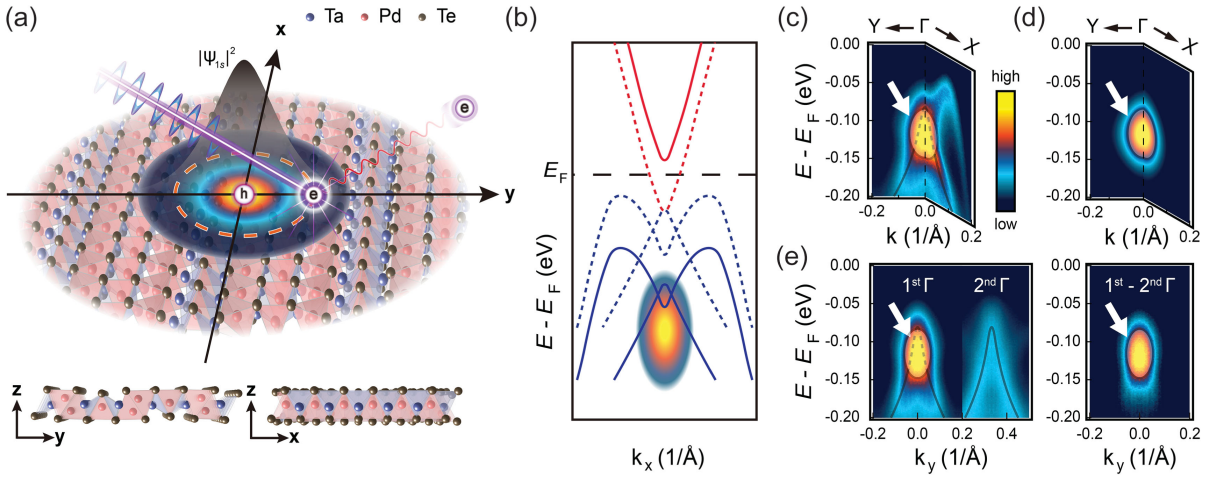


FIG. 1. (a) An experimental setup of exciton photoemission with linearly polarized light. The squared exciton radial wave function simulated with experimental parameters are plot over the schematic model of the surface layer of $Ta_2Pd_3Te_5$. See text for the simulation procedure. Side views of the layer are given at the bottom. (b) A schematic band structure of $Ta_2Pd_3Te_5$ around the Fermi energy (E_F) along k_x. The solid (dashed) lines represent the bands below (above) T_c. The simulated momentum distribution of excitons is plot together. (c) ARPES spectra of $Ta_2Pd_3Te_5$ along the $\Gamma - Y$ ($\Gamma - X$) direction. (d) The exciton photoemission spectral function simulated from the ARPES spectra in (c). [the left column in (e)] ARPES spectra along $\Gamma - Y$ taken with xz polarization at the centers of the first and the second BZs. Right: the difference of the two spectra is shown clearly by the subtraction after normalization, which corresponds to the pure exciton photoemission signal.

insulating ground state of a solid as well as the excitonic insulator nature of Ta_2NiSe_5 elusive.

In this context, we focus on another, very recent, excitonic insulator candidate material $Ta_2Pd_3Te_5$ [45–49]. While $Ta_2Pd_3Te_5$ has a similar band structure and a similar gap-opening transition ($T_c = 365$ K) with Ta_2NiSe_5, its structural distortion is undetectably small in x-ray diffraction [45,46,49] with only signatures of symmetry breaking in electron diffraction [46,49] and scanning tunneling microscopy (See Fig. S1 in Ref. [50], which includes Refs. [51,53]). This unique property positions $Ta_2Pd_3Te_5$ as an unprecedentedly promising candidate for an excitonic insulator with the excitonic coupling dominating over the electron-lattice coupling. Nevertheless, the clear evidence for excitons within the insulating phase has not been available. Here, we identify the exciton photoemission signal from the insulating phase of this material using ARPES, confirming the existence of excitons in a ground state of a crystal. The detailed properties of the excitons formed, which cannot be probed by other experimental probes, are investigated to reveal the size and the unusual odd parity of excitons in this material.

$Ta_2Pd_3Te_5$ is a layered material and its single layer is composed of unit cells with multiple Ta and Pd chains [Fig. 1(a), see Appendix A for the details of the crystal growth]. The chain structure gives rise to semimetallic band dispersions along the chains and flat bands across the chains. Its butterfly-shape valence bands along k_x [Fig. 1(b)] come from Pd d_{xz} and Te p_x orbitals and the parabolic conduction band from Ta d_{z^2} electrons [46,47,54]. These bands degenerate at the center of the Brillouin zone (BZ) (Γ) to make a zero-gap semimetal in the normal state, which are well reproduced in the band calculations using density functional theory (DFT) [46,48,49]. Because of the mirror symmetry inherent in the atomic and orbital structures, each band exhibits a pronounced polarization dependence (see Figs. S4 and S5 in Ref. [50] and Appendix B for details) [44]. The valence (conduction) band spectral weight is suppressed in ARPES spectra taken at $yz(x)$ polarization shown in Fig. 2(c) [Fig. 2(d)] along $\Gamma - X$ due to their orbital characters [see also Fig. S5a and Eq. (S5b) in Ref. [50] for detail]. A metal-insulator transition starts from 365 K as the valence (conduction) bands move gradually to a lower energy (higher above the Fermi level) as shown in Fig. 2 (see also Figs. S6 and S7 in Ref. [50] for detail). The band gap becomes obvious below 300 K beyond the energy broadening of ARPES spectra [Figs. 2(c) and 2(f)]. Temperature-dependent band dispersions are fully consistent with the recent ARPES works [45,46,49]. The structural investigation within those works further found a structural symmetry breaking with marginal distortions. The band gap expected in the DFT calculations is, however, on the order of a few meV so that an extra many-body interaction is needed to explain the observed band gap of ~100 meV (see Fig. S8 in Ref. [50] and Appendix C for details). The existence of any extra charge density wave is excluded in the structural studies [46,49] and the scanning tunneling microscopy measurement (See Fig. S1 in Ref. [50]). Moreover, the strong correlation effect is not likely since the gap forms from a highly dispersing Dirac band.

The ARPES spectra in Fig. 1(c) combine those obtained along high-symmetry lines of the BZ, $\Gamma - Y$ and $\Gamma - X$, in

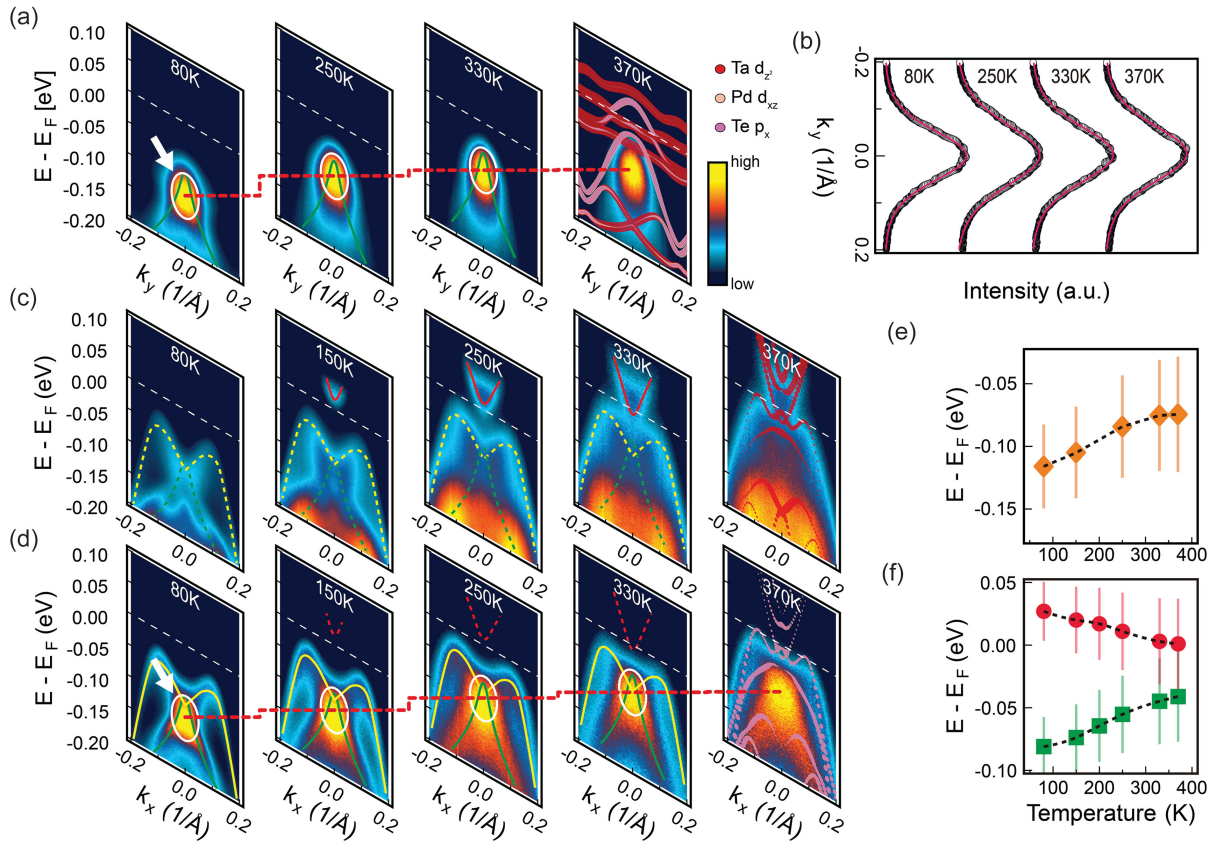


FIG. 2. (a) ARPES spectra taken along the $\Gamma - Y$ direction exhibits the evolution of the exciton photoemission as a function of temperature with the valence band photoemission. (b) MDCs (dots) crossing the maximum spectral weights from (a) and their fits (pink lines) by the exciton wave functions. (c) Temperature-dependent ARPES spectra (divided by Fermi Dirac functions) obtained along $\Gamma - X$ with yz polarization. The band gap evolution is very clear. (d) Temperature-dependent ARPES spectra along $\Gamma - X$ obtained with x polarization. The calculated band structure for the normal phase are overlaid over the 370 K spectra in (a),(c), and (d) with the orbital contributions resolved. (e) The shifts of exciton photoemission peak as a function of temperature, and they are extracted from the Γ point of xz-polarized ARPES results. (f) The shifts of the conduction (red) and valence (green) band edges as a function of temperature exhibiting the gradual opening of the band gap upon cooling. The conduction and valence bands are extracted from the Γ point of yz- and xz-polarized ARPES results, respectively.

the insulating phase at 80 K. One can immediately notice a strong and unusual photoemission signal at the Γ point below the valence band maximum located at -0.08 eV [schematics in Fig. 1(b) and see Fig. S9 in Ref. [50] for more details]. This signal deviates largely from the valence band dispersions, both calculated and measured ones, shown in Figs. 2(a), 2(c), and 2(d) [46,47,54]. Moreover, it disappears completely in the second BZ as shown in Fig. 1(e), where the bare valence band signals persist. Note also that the valence band dispersion changes dramatically from $\Gamma - X$ to $\Gamma - Y$ while the spectral feature at Γ is consistent. It is thus unambiguous that this signal does not come from valence bands. To quantify this unusual spectral function, we subtracted the ARPES spectra of the first BZ by the bare valence band spectra obtained in the second BZ, which is given on the right panel of Fig. 1(e) (see Fig. S9 in Ref. [50] for detail). The spectral function subtracted is largely isotropic in momentum but slightly squeezed along the $\Gamma - Y$ direction [Fig. 1(c) and see Fig. S9 in Ref. [50] for details]. The unusual spectral shape in energy and momentum is not compatible with spectra features due to electron-phonon interactions such as polaronic sidebands and shake-up replica of the valence band [55–60]. The fluctuation- or temperature-induced spectral broadening cannot explain this spectral distribution, since it is consistent down to a very low temperature of 10 K (see Fig. S12 in Ref. [50] for detail). We further excluded the phonon broadening of the valence band by quantitatively simulating the spectral function using a two-band Bethe-Salpeter equation and phonon-induced replica bands (see Figs. S10 and S11 in Ref. [50] for detail). It was also reported that the top of the valence band has no k_z dispersion, which rules out any substantial final state effect to broaden the spectra at Γ [61].

However, this egg-shape photoemission signal is remarkably similar to the spectral function of the exciton photoemission observed previously [34–44,62]. This signal can be simulated quantitatively well by the exciton

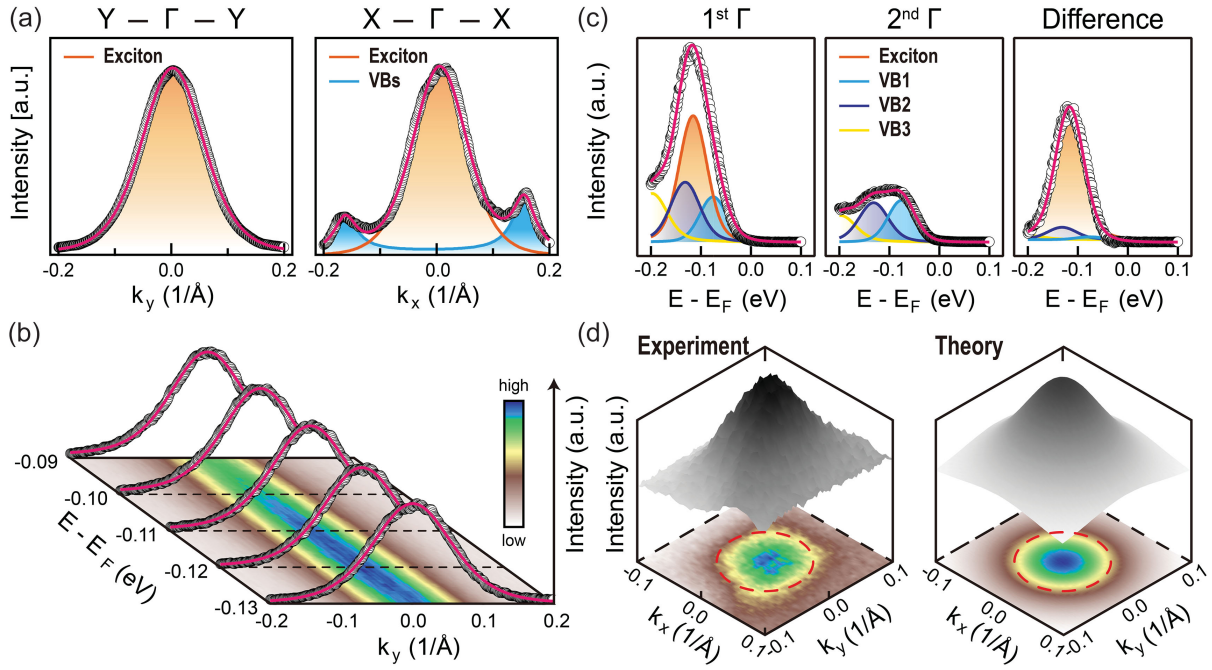


FIG. 3. (a) MDCs crossing the maximum spectral weights from the spectra shown in Fig. 1(c) (circles) are fit by the exciton wave function (pink lines). (b) Energy dependence of the fits (pink lines) of exciton wave function for the MDCs (circles) obtained for the ARPES spectrum along $\Gamma - Y$ direction (xz polarization) at 80 K. (c) Fits for EDCs from the spectra and its difference shown in Fig. 1(e). [(d), left] ARPES momentum distribution map obtained from the x-polarized photon at the peak position of exciton photoemission (−0.115 eV). Right: 2D distribution of exciton wave function obtained from fittings of the experimental map in the left.

photoemission formula [Figs. 1(d) and 3(d)] with the exciton wave function and the valence band dispersions at the Γ point [43,44]. The exciton wave function was extracted by fitting the momentum distribution curves [MDCs, Figs. 3(a) and 3(b)] of the subtracted spectra along both $\Gamma - Y$ (left) and $\Gamma - X$ (right) (see the Tables in Ref. [50] for the fitting parameters). The wave function corresponds to an $1s$ wave function, which exhibits a slightly larger Bohr radius along the $\Gamma - X$ direction (approximately 15.1 Å) than along $\Gamma - Y$ (approximately 13.6 Å) due to the marginal anisotropy mentioned above. The anisotropic shape of the exciton seems to reflect the anisotropic band structure [44]. The angular distribution of the exciton wave function [Fig. 3(d)] is consistent with the recent result of tight-binding calculations of excitons in a $Ta_2Pd_3Te_5$ monolayer [47] while the calculation predicts two times larger exciton radius. The energy distribution curves (EDCs) at Γ are fitted by Voigt functions as illustrated in Fig. 3(c), which shows an energy broadening of approximately 0.1 eV. This reflects the scattering of excitons, which is thought to be due mainly to phonons [63].

The temperature-dependent ARPES measurements shown in Fig. 2 (see also Figs. S12 and S13 in Ref. [50] for detail) show that the exciton photoemission signal remains robust below T_c [Fig. 2(a)]. However, the excitonic signal moves systematically to a lower energy [Figs. 2(a) and 2(e)] with rising temperature, which is consistently lower than the valence band top. Namely, the exciton binding energy surpasses the band gap enough to drive the metal-insulator transition in the whole temperature range below T_c. In addition, a gradual spectral weight transfer is observed from the valence band to the exciton photoemission feature during the transition (see also Fig. S14 in Ref. [50] for detail). In clear contrast, the exciton photoemission in Ta_2NiSe_5 was observed only above T_c [44]. This suggests that the observed excitons in Ta_2NiSe_5 are incoherent excitons preformed above the condensation temperature and the excitonic transition is near the crossover of a Bose-Einstein condensation [46,49,64–66]. The present experimental setup did not allow us to reach a temperature above 400 K so that the existence of preformed excitons in $Ta_2Pd_3Te_5$ is not clear. The reason for the loss of the exciton photoemission below T_c in Ta_2NiSe_5 is not understood yet but may be related to the strong electron-lattice and exciton-lattice interactions [32,33,44,67,68].

A further contrasting property of the exciton photoemission can be found in its polarization dependence, which is dictated by the photoemission dipole selection rule. The exciton photoemission signal is a product of the s-wave-like exciton envelope and the photoemission matrix element from the conduction band orbital [43,44]. The exciton feature in Ta_2NiSe_5 was found to have even parity for both mirror planes as selectively probed by z-polarized photons [44]. In contrast, the present exciton photoemission signal is clearly observed for x-polarized photons but

suppressed in the yz polarization [Fig. 2(c)], indicating a contribution of an odd parity wave function along the yz plane (see Figs. S4 and S15 in Ref. [50] for detail). We note that the only odd parity wave function involved here is the valence Pd d_{xy} orbital [Fig. 2(d)], which is not expected to contribute to the photoemission from a conventional excited-state exciton within a band gap. However, the strong mixing of the valence and conduction bands near Γ is natural in an excitonic insulator [11,46,49], which allows the valence band orbital to contribute to the exciton photoemission matrix element. The interband hybridization is allowed by or induces the structural symmetry breaking mentioned above. Then, the distinct parity of exciton spectral functions in Ta_2NiSe_5 and the present crystal is also straightforwardly explained by the difference in the orbital parity of their valence orbitals; Ta_2NiSe_5's valence band has even parity for both the x and y axes.

In summary, we detected a characteristic photoemission signal from excitons in an emerging insulating state of a 3D crystalline solid, $Ta_2Pd_3Te_5$, which evidences the excitonic insulator nature of the insulating state. The exciton binding energy was tracked throughout the gradual gap opening transition and the symmetry and the envelope of exciton wave function were determined. The nearly distortion-less nature of the transition and the highest T_c makes this system an ideal platform to exploit exciton condensates in a bulk solid. The symmetry-broken, odd-parity, nature of the excitons observed may lead to discovering exotic many-body quantum states [52,69] under the nontrivial topological nature of the present system [54,61,70–72].

Acknowledgments—This work was supported by the Institute for Basic Science (Grant No. IBS-R014-D1). K.-H. J. was supported by Global-Learning & Academic research institution for Master's·PhD students, and Postdocs (LAMP) Program of the National Research Foundation of Korea (NRF) funded by the Ministry of Education (Grant No. RS-2024-00443714). C. W. was supported by NRF research grant (No. RS-2022-NR068223). S-W. C. was supported by the W. M. Keck Foundation grant to the Keck Center for Quantum Magnetism at Rutgers University.

Data availability—The data that support the findings of this Letter are openly available [73].

[1] H. Van Amerongen, R. Van Grondelle *et al.*, *Photosynthetic Excitons* (World Scientific, Singapore, 2000).
[2] T. Brixner, J. Stenger, H. M. Vaswani, M. Cho, R. E. Blankenship, and G. R. Fleming, Two-dimensional spectroscopy of electronic couplings in photosynthesis, Nature (London) **434**, 625 (2005).
[3] Y. Kuznetsova, M. Remeika, A. High, A. Hammack, L. Butov, M. Hanson, and A. Gossard, All-optical excitonic transistor, Opt. Lett. **35**, 1587 (2010).
[4] S. M. Menke, W. A. Luhman, and R. J. Holmes, Tailored exciton diffusion in organic photovoltaic cells for enhanced power conversion efficiency, Nat. Mater. **12**, 152 (2013).
[5] E. Romero, R. Augulis, V. I. Novoderezhkin, M. Ferretti, J. Thieme, D. Zigmantas, and R. Van Grondelle, Quantum coherence in photosynthesis for efficient solar-energy conversion, Nat. Phys. **10**, 676 (2014).
[6] J. S. Ross, P. Klement, A. M. Jones, N. J. Ghimire, J. Yan, D. Mandrus, T. Taniguchi, K. Watanabe, K. Kitamura, W. Yao *et al.*, Electrically tunable excitonic light-emitting diodes based on monolayer WSe_2 p–n junctions, Nat. Nanotechnol. **9**, 268 (2014).
[7] M. M. Furchi, A. Pospischil, F. Libisch, J. Burgdorfer, and T. Mueller, Photovoltaic effect in an electrically tunable van der Waals heterojunction, Nano Lett. **14**, 4785 (2014).
[8] Y. Ye, Z. J. Wong, X. Lu, X. Ni, H. Zhu, X. Chen, Y. Wang, and X. Zhang, Monolayer excitonic laser, Nat. Photonics **9**, 733 (2015).
[9] E. Romero, V. I. Novoderezhkin, and R. Van Grondelle, Quantum design of photosynthesis for bio-inspired solar-energy conversion, Nature (London) **543**, 355 (2017).
[10] T. Mueller and E. Malic, Exciton physics and device application of two-dimensional transition metal dichalcogenide semiconductors, npj 2D Mater. Appl. **2**, 29 (2018).
[11] D. Jérome, T. Rice, and W. Kohn, Excitonic insulator, Phys. Rev. **158**, 462 (1967).
[12] B. Halperin and T. Rice, Possible anomalies at a semimetal-semiconductor transistion, Rev. Mod. Phys. **40**, 755 (1968).
[13] Y. Wakisaka, T. Sudayama, K. Takubo, T. Mizokawa, M. Arita, H. Namatame, M. Taniguchi, N. Katayama, M. Nohara, and H. Takagi, Excitonic insulator state in Ta_2NiSe_5 probed by photoemission spectroscopy, Phys. Rev. Lett. **103**, 026402 (2009).
[14] T. Pillo, J. Hayoz, H. Berger, F. Lévy, L. Schlapbach, and P. Aebi, Photoemission of bands above the Fermi level: The excitonic insulator phase transition in 1T-$TiSe_2$, Phys. Rev. B **61**, 16213 (2000).
[15] K. Seki, Y. Wakisaka, T. Kaneko, T. Toriyama, T. Konishi, T. Sudayama, N. Saini, M. Arita, H. Namatame, M. Taniguchi *et al.*, Excitonic Bose-Einstein condensation in Ta_2NiSe_5 above room temperature, Phys. Rev. B **90**, 155116 (2014).
[16] K. Sugawara, Y. Nakata, R. Shimizu, P. Han, T. Hitosugi, T. Sato, and T. Takahashi, Unconventional charge-density-wave transition in monolayer 1T-$TiSe_2$, ACS Nano **10**, 1341 (2016).
[17] A. Kogar, M. S. Rak, S. Vig, A. A. Husain, F. Flicker, Y. I. Joe, L. Venema, G. J. MacDougall, T. C. Chiang, E. Fradkin *et al.*, Signatures of exciton condensation in a transition metal dichalcogenide, Science **358**, 1314 (2017).
[18] Y. Song, C. Jia, H. Xiong, B. Wang, Z. Jiang, K. Huang, J. Hwang, Z. Li, C. Hwang, Z. Liu *et al.*, Signatures of the exciton gas phase and its condensation in monolayer 1T-$ZrTe_2$, Nat. Commun. **14**, 1116 (2023).
[19] Q. Gao, Y.-h. Chan, Y. Wang, H. Zhang, P. Jinxu, S. Cui, Y. Yang, Z. Liu, D. Shen, Z. Sun *et al.*, Evidence of high-temperature exciton condensation in a two-dimensional semimetal, Nat. Commun. **14**, 994 (2023).
[20] Q. Gao, Y.-h. Chan, P. Jiao, H. Chen, S. Yin, K. Tangprapha, Y. Yang, X. Li, Z. Liu, D. Shen *et al.*, Observation of

possible excitonic charge density waves and metal–insulator transitions in atomically thin semimetals, Nat. Phys. **20**, 597 (2024).
[21] Y. H. Kwan, T. Devakul, S. Sondhi, and S. Parameswaran, Theory of competing excitonic orders in insulating WTe_2 monolayers, Phys. Rev. B **104**, 125133 (2021).
[22] Y. Jia, P. Wang, C.-L. Chiu, Z. Song, G. Yu, B. Jäck, S. Lei, S. Klemenz, F. A. Cevallos, M. Onyszczak *et al.*, Evidence for a monolayer excitonic insulator, Nat. Phys. **18**, 87 (2022).
[23] B. Sun, W. Zhao, T. Palomaki, Z. Fei, E. Runburg, P. Malinowski, X. Huang, J. Cenker, Y.-T. Cui, J.-H. Chu *et al.*, Evidence for equilibrium exciton condensation in monolayer WTe_2, Nat. Phys. **18**, 94 (2022).
[24] Y. Que, Y.-H. Chan, J. Jia, A. Das, Z. Tong, Y.-T. Chang, Z. Cui, A. Kumar, G. Singh, S. Mukherjee *et al.*, A gate-tunable ambipolar quantum phase transition in a topological excitonic insulator, Adv. Mater. **36**, 2309356 (2024).
[25] K. Rossnagel, L. Kipp, and M. Skibowski, Charge-density-wave phase transition in 1T-$TiSe_2$: Excitonic insulator versus band-type Jahn-Teller mechanism, Phys. Rev. B **65**, 235101 (2002).
[26] M. Porer, U. Leierseder, J.-M. Ménard, H. Dachraoui, L. Mouchliadis, I. Perakis, U. Heinzmann, J. Demsar, K. Rossnagel, and R. Huber, Non-thermal separation of electronic and structural orders in a persisting charge density wave, Nat. Mater. **13**, 857 (2014).
[27] A. Wegner, J. Zhao, J. Li, J. Yang, A. Anikin, G. Karapetrov, K. Esfarjani, D. Louca, and U. Chatterjee, Evidence for pseudo–Jahn-Teller distortions in the charge density wave phase of 1T-$TiSe_2$, Phys. Rev. B **101**, 195145 (2020).
[28] D. Jeong, J. Kim, K.-H. Jin, J. Kim, and H. W. Yeom, Dichotomy of metallic electron density and charge density wave in 1T-$TiSe_2$, Phys. Rev. B **109**, 125117 (2024).
[29] M. D. Watson, I. Marković, E. A. Morales, P. Le Fèvre, M. Merz, A. A. Haghighirad, and P. D. C. King, Band hybridization at the semimetal-semiconductor transition of Ta_2NiSe_5 enabled by mirror-symmetry breaking, Phys. Rev. Res. **2**, 013236 (2020).
[30] L. Windgätter, M. Rösner, G. Mazza, H. Hübener, A. Georges, A. J. Millis, S. Latini, and A. Rubio, Common microscopic origin of the phase transitions in Ta_2NiS_5 and the excitonic insulator candidate Ta_2NiSe_5, npj Comput. Mater. **7**, 210 (2021).
[31] H. Lu, M. Rossi, J.-h. Kim, H. Yavas, A. Said, A. Nag, M. Garcia-Fernandez, S. Agrestini, K.-J. Zhou, C. Jia *et al.*, Evolution of the electronic structure in Ta_2NiSe_5 across the structural transition revealed by resonant inelastic x-ray scattering, Phys. Rev. B **103**, 235159 (2021).
[32] T. Kaneko, T. Toriyama, T. Konishi, and Y. Ohta, Orthorhombic-to-monoclinic phase transition of Ta_2NiSe_5 induced by the Bose-Einstein condensation of excitons, Phys. Rev. B **87**, 035121 (2013).
[33] G. Mazza, M. Rösner, L. Windgätter, S. Latini, H. Hübener, A. J. Millis, A. Rubio, and A. Georges, Nature of symmetry breaking at the excitonic insulator transition: Ta_2NiSe_5, Phys. Rev. Lett. **124**, 197601 (2020).
[34] G. D. Scholes and G. Rumbles, Excitons in nanoscale systems, Nat. Mater. **5**, 683 (2006).
[35] X. Cui, C. Wang, A. Argondizzo, S. Garrett-Roe, B. Gumhalter, and H. Petek, Transient excitons at metal surfaces, Nat. Phys. **10**, 505 (2014).
[36] T. Byrnes, N. Y. Kim, and Y. Yamamoto, Exciton–polariton condensates, Nat. Phys. **10**, 803 (2014).
[37] H. Tanimura, K. Tanimura, and P. H. M. Van Loosdrecht, Dynamics of incoherent exciton formation in Cu_2O: Time- and angle-resolved photoemission spectroscopy, Phys. Rev. B **100**, 115204 (2019).
[38] J. Madéo, M. K. Man, C. Sahoo, M. Campbell, V. Pareek, E. L. Wong, A. Al-Mahboob, N. S. Chan, A. Karmakar, B. M. K. Mariserla *et al.*, Directly visualizing the momentum-forbidden dark excitons and their dynamics in atomically thin semiconductors, Science **370**, 1199 (2020).
[39] M. K. Man, J. Madéo, C. Sahoo, K. Xie, M. Campbell, V. Pareek, A. Karmakar, E. L. Wong, A. Al-Mahboob, N. S. Chan *et al.*, Experimental measurement of the intrinsic excitonic wave function, Sci. Adv. **7**, eabg0192 (2021).
[40] O. Karni, E. Barré, V. Pareek, J. D. Georgaras, M. K. Man, C. Sahoo, D. R. Bacon, X. Zhu, H. B. Ribeiro, A. L. O'Beirne *et al.*, Structure of the moiré exciton captured by imaging its electron and hole, Nature (London) **603**, 247 (2022).
[41] R. Mori, S. Ciocys, K. Takasan, P. Ai, K. Currier, T. Morimoto, J. E. Moore, and A. Lanzara, Spin-polarized spatially indirect excitons in a topological insulator, Nature (London) **614**, 249 (2023).
[42] V. Pareek, D. R. Bacon, X. Zhu, Y.-H. Chan, F. Bussolotti, N. S. Chan, J. P. Urquizo, K. Watanabe, T. Taniguchi, M. K. Man *et al.*, Driving non-trivial quantum phases in conventional semiconductors with intense excitonic fields, arXiv:2403.08725.
[43] A. Rustagi and A. F. Kemper, Photoemission signature of excitons, Phys. Rev. B **97**, 235310 (2018).
[44] K. Fukutani, R. Stania, C. Il Kwon, J. S. Kim, K. J. Kong, J. Kim, and H. W. Yeom, Detecting photoelectrons from spontaneously formed excitons, Nat. Phys. **17**, 1024 (2021).
[45] M. S. Hossain, T. A. Cochran, Y.-X. Jiang, S. Zhang, H. Wu, X. Liu, X. Zheng, B. Kim, G. Cheng, Q. Zhang *et al.*, Discovery of a topological exciton insulator with tunable momentum order, arXiv:2312.15862.
[46] J. Huang, B. Jiang, J. Yao, D. Yan, X. Lei, J. Gao, Z. Guo, F. Jin, Y. Li, Z. Yuan *et al.*, Evidence for an excitonic insulator state in $Ta_2Pd_3Te_5$, Phys. Rev. X **14**, 011046 (2024).
[47] J. Yao, H. Sheng, R. Zhang, R. Pang, J.-J. Zhou, Q. Wu, H. Weng, X. Dai, Z. Fang, and Z. Wang, Excitonic instability in $Ta_2Pd_3Te_5$ monolayer, Chin. Phys. Lett. **41**, 097101 (2024).
[48] B. Jiang, J. Yao, D. Yan, Z. Guo, G. Qu, X. Deng, Y. Huang, H. Ding, Y. Shi, Z. Wang *et al.*, Surface doping manipulation of the insulating ground states in $Ta_2Pd_3Te_5$ and $Ta_2Ni_3Te_5$, Chin. Phys. B **33**, 067402 (2024).
[49] P. Zhang, Y. Dong, D. Yan, B. Jiang, T. Yang, J. Li, Z. Guo, Y. Huang, Q. Li, Y. Li *et al.*, Spontaneous gap opening and potential excitonic states in an ideal Dirac semimetal $Ta_2Pd_3Te_5$, Phys. Rev. X **14**, 011047 (2024).
[50] See Supplemental Material at http://link.aps.org/supplemental/10.1103/5kd3-trkg for additional data and calculated results, which includes Refs. [11,43–46,49,51,52].

[51] P. Zhang, P. Richard, T. Qian, Y.-M. Xu, X. Dai, and H. Ding, A precise method for visualizing dispersive features in image plots, Rev. Sci. Instrum. **82** (2011).
[52] R. Wang, O. Erten, B. Wang, and D. Xing, Prediction of a topological p + ip excitonic insulator with parity anomaly, Nat. Commun. **10**, 210 (2019).
[53] T. Kaneko and Y. Ohta, A new era of excitonic insulators, J. Phys. Soc. Jpn. **94**, 012001 (2025).
[54] X. Wang, D. Geng, D. Yan, W. Hu, H. Zhang, S. Yue, Z. Sun, S. Kumar, E. F. Schwier, K. Shimada *et al.*, Observation of topological edge states in the quantum spin Hall insulator $Ta_2Pd_3Te_5$, Phys. Rev. B **104**, L241408 (2021).
[55] C. Chen, J. Avila, E. Frantzeskakis, A. Levy, and M. C. Asensio, Observation of a two-dimensional liquid of Fröhlich polarons at the bare $SrTiO_3$ surface, Nat. Commun. **6**, 8585 (2015).
[56] M. Kang, S. W. Jung, W. J. Shin, Y. Sohn, S. H. Ryu, T. K. Kim, M. Hoesch, and K. S. Kim, Holstein polaron in a valley-degenerate two-dimensional semiconductor, Nat. Mater. **17**, 676 (2018).
[57] J. M. Riley, F. Caruso, C. Verdi, L. Duffy, M. D. Watson, L. Bawden, K. Volckaert, G. Van Der Laan, T. Hesjedal, M. Hoesch *et al.*, Crossover from lattice to plasmonic polarons of a spin-polarised electron gas in ferromagnetic EuO, Nat. Commun. **9**, 2305 (2018).
[58] G. Antonius, Y.-H. Chan, and S. G. Louie, Polaron spectral properties in doped ZnO and $SrTiO_3$ from first principles, Phys. Rev. Res. **2**, 043296 (2020).
[59] F. Caruso, P. Amsalem, J. Ma, A. Aljarb, T. Schultz, M. Zacharias, V. Tung, N. Koch, and C. Draxl, Two-dimensional plasmonic polarons in n-doped monolayer MoS_2, Phys. Rev. B **103**, 205152 (2021).
[60] L. Kang, X. Du, J. Zhou, X. Gu, Y. Chen, R. Xu, Q. Zhang, S. Sun, Z. Yin, Y. Li *et al.*, Band-selective Holstein polaron in Luttinger liquid material $A_{0.3}MoO_3$ (A = K, Rb), Nat. Commun. **12**, 6183 (2021).
[61] A. Wang, Y. Li, G. Yang, D. Yan, Y. Huang, Z. Guo, J. Gao, J. Huang, Q. Zeng, D. Qian *et al.*, A robust and tunable Luttinger liquid in correlated edge of transition-metal second-order topological insulator $Ta_2Pd_3Te_5$, Nat. Commun. **14**, 7647 (2023).
[62] D. Christiansen, M. Selig, E. Malic, R. Ernstorfer, and A. Knorr, Theory of exciton dynamics in time-resolved ARPES: Intra-and intervalley scattering in two-dimensional semiconductors, Phys. Rev. B **100**, 205401 (2019).
[63] L. Ni, U. Huynh, A. Cheminal, T. H. Thomas, R. Shivanna, T. F. Hinrichsen, S. Ahmad, A. Sadhanala, and A. Rao, Real-time observation of exciton–phonon coupling dynamics in self-assembled hybrid perovskite quantum wells, ACS Nano **11**, 10834 (2017).
[64] Y. Lu, H. Kono, T. Larkin, A. Rost, T. Takayama, A. Boris, B. Keimer, and H. Takagi, Zero-gap semiconductor to excitonic insulator transition in Ta_2NiSe_5, Nat. Commun. **8**, 14408 (2017).
[65] K. Okazaki, Y. Ogawa, T. Suzuki, T. Yamamoto, T. Someya, S. Michimae, M. Watanabe, Y. Lu, M. Nohara, H. Takagi *et al.*, Photo-induced semimetallic states realised in electron–hole coupled insulators, Nat. Commun. **9**, 4322 (2018).
[66] D. Werdehausen, T. Takayama, G. Albrecht, Y. Lu, H. Takagi, and S. Kaiser, Photo-excited dynamics in the excitonic insulator Ta_2NiSe_5, J. Phys. Condens. Matter **30**, 305602 (2018).
[67] C. Chen, X. Chen, W. Tang, Z. Li, S. Wang, S. Ding, Z. Kang, C. Jozwiak, A. Bostwick, E. Rotenberg *et al.*, Role of electron-phonon coupling in excitonic insulator candidate Ta_2NiSe_5, Phys. Rev. Res. **5**, 043089 (2023).
[68] C. Chen, W. Tang, X. Chen, Z. Kang, S. Ding, K. Scott, S. Wang, Z. Li, J. P. Ruff, M. Hashimoto *et al.*, Anomalous excitonic phase diagram in band-gap-tuned $Ta_2Ni(Se,S)_5$, Nat. Commun. **14**, 7512 (2023).
[69] V. Kozii and L. Fu, Odd-parity superconductivity in the vicinity of inversion symmetry breaking in spin-orbit-coupled systems, Phys. Rev. Lett. **115**, 207002 (2015).
[70] Z. Guo, D. Yan, H. Sheng, S. Nie, Y. Shi, and Z. Wang, Quantum spin Hall effect in $Ta_2M_3Te_5$ (M = Pd, Ni), Phys. Rev. B **103**, 115145 (2021).
[71] Y. Li, D. Yan, Y. Hong, H. Sheng, A. Wang, Z. Dou, X. Guo, X. Shi, Z. Su, Z. Lyu *et al.*, Interfering Josephson diode effect in $Ta_2Pd_3Te_5$ asymmetric edge interferometer, Nat. Commun. **15**, 9031 (2024).
[72] H. Yu, D. Yan, Z. Guo, Y. Zhou, X. Yang, P. Li, Z. Wang, X. Xiang, J. Li, X. Ma *et al.*, Observation of emergent superconductivity in the topological insulator $Ta_2Pd_3Te_5$ via pressure manipulation, J. Am. Chem. Soc. **146**, 3890 (2024).
[73] Siwon Lee, Han Woong Yeom *et al.*, Replication data for: Exciton photoemission from a ground state of a solid Ta2Pd3Te5, Harvard Dataverse, 10.7910/DVN/AHP3TC (2025).
[74] G. Kresse and J. Furthmüller, Efficient iterative schemes for *ab initio* total-energy calculations using a plane-wave basis set, Phys. Rev. B **54**, 11169 (1996).
[75] J. P. Perdew, K. Burke, and M. Ernzerhof, Generalized gradient approximation made simple, Phys. Rev. Lett. **77**, 3865 (1996).

End Matter

Appendix A: Crystal growth—Single crystals of $Ta_2Pd_3Te_5$ were synthesized using the self-flux method. A mixture of Ta (powder, 99.999%), Pd (powder, 99.9999%), and Te (lump, 99.9999%) in a molar ratio of 2.0:4.5:7.5 (Ta:Pd:Te) was prepared in an argon-filled glove box. The mixture was placed in an alumina crucible, sealed in an evacuated quartz tube, and heated to 950 °C over a period of 10 hours. It was then maintained at this temperature for 2 days. Following this, the tube was cooled to 800 °C at a rate of 0.5 °C/h. The crystalline quality was confirmed by x-ray diffraction and spectroscopy (see Figs. S2 and S3 in Ref. [50] for detail).

Appendix B: ARPES experiment—All ARPES experiments were performed using the DA-30L electron

analyzer (Scienta Omicron, Sweden) and a laser of photon energy 11 eV (Oxide, Japan). The typical energy resolution was better than 0.6 meV. $Ta_2Pd_3Te_5$ single crystal was cleaved at 75–80 K in ultrahigh vacuum ($\sim 10^{-11}$ torr) before measurements.

Appendix C: DFT calculation—The first-principles calculations were performed within the framework of the density functional theory (DFT) using the Perdew-Burke-Ernzerhof-type generalized gradient approximation for the exchange-correlation functional, as implemented in the Vienna *ab initio* simulation package [74,75]. In the self-consistent process, all the calculations were carried out using the kinetic energy cutoff of 520 eV on a $15 \times 5 \times 4$ Monkhorst-Pack k-point mesh for the $Ta_2Pd_3Te_5$ bulk and a $15 \times 5 \times 1$ for the slab calculations. The spin-orbit coupling effect was included in the self-consistent electronic structure calculation. The lattice constants were taken from experiments [54], but the atoms in the unit cell are fully relaxed with the force cutoff of $0.01\ \mathrm{eV\,\AA^{-1}}$. The electronic self-consistent iteration was converged to 10^{-5} eV precision of the total energy.